E21

A Porous Bulk Metallic Glass with Unidirectional Opening Pores

X. H. Chen,[a] Y. Zhang,[a,z] X. C. Zhang,[a] X. D. Hui,[a] B. C. Wei,[b] and G. L. Chen[a]

[a]*State Key Laboratory for Advanced Metals and Materials, University of Science and Technology Beijing, Beijing 100083, China*
[b]*National Microgravity Laboratory, Institute of Mechanics, Chinese Academy of Sciences, Beijing 100080, China*

Porous Zr-based bulk metallic glass (PMG) with unidirectional opening pores is prepared by electrochemical etching of tungsten wires of the W/bulk metallic glass (BMG) composites. The porosity and pore size can be controlled by adjusting the tungsten wires. The PMG showed no measurable loss in thermal stability as compared to the monolithic Zr-based BMG by water quenching and is more ductile and softer than the pore-free counterpart. The specific surface area of the PMGs is calculated to be 0.65, 3.96, and 10.54 m^2/kg for 20, 60, and 80 vol % porosity, respectively.

© 2007 The Electrochemical Society. [DOI: 10.1149/1.2787868] All rights reserved.

Porous metallic glass (PMG) materials have received increasing interest in recent years because they combine the advantages of metallic foams and metallic glasses.[1-8] Metallic foam materials exhibit properties like high specific strength and high energy-absorption capacity,[9] whereas metallic glasses have distinctive characteristics like high strength, wear resistance, and strong corrosion resistance combined with desirable properties at relatively low densities.[10] Thus, PMGs may find possible applications as fluid filters, catalytic substrates, and biomedical implants.[1,2]

Most of the processing technique for PMG is a replication or reformation method used previously in the production of crystalline metal foams,[1-8] and they can be divided into two groups: liquid state/supercooled liquid state processing and solid-state processing. For the first case, pores of metallic glasses were made under liquid state and supercooled liquid state with the aid of some pore-formers, such as gas-generating flux additives,[3] soluble place holders,[4,5] and hollow carbonspheres.[6] These techniques all require that the metallic glass systems have a high glass-forming ability to allow synthesis of the final PMG, as the introduction of pores during foaming decreases thermal conductivity of the melt. Some new porous forming techniques for metallic glass foaming by means of solid-state processing have also been developed. For example, a porous Ti-based metallic glass has been fabricated by applying the principle of selective phase dissolution in $Y_{20}Ti_{36}Al_{24}Co_{20}$ two-phase amorphous alloy,[7] and Lee et al. synthesized uniformly distributed nanoscale pores within a $Cu_{47}Ti_{33}Zr_{11}Ni_8Si_1$ metallic glass by extruding layered Cu-based metallic glass + Cu composite powders following dissolution of the Cu in a HNO_3 solution.[8]

Until now, the PMGs prepared by the above-mentioned methods have contained a disordered pore structure. Materials with unidirectional opening pores may have some special potential application in the fields of engineering, electronics, photonics, and life sciences.[11] For porous crystalline metals, Higuchi et al. reported the biocompatibility of lotus-type porous stainless and titanium in alveolar bone in order to investigate the possibility of an implant by animal experiments, then concluded that titanium can be utilized to create pores of 150–200 μm in diameter which would allow growth of bony tissues alone in the pores to enhance holding force.[12] In the current study, we report the fabrication of porous $Zr_{47}Ti_{13}Cu_{11}Ni_{10}Be_{16}Nb_3$ bulk metallic glasses (BMGs) with uniformly dispersed unidirectional pores by sequential processes. The alloy is only a model one which can be changed to some other commercial BMG alloy, like Vit106 ($Zr_{57}Nb_5Cu_{15.4}Ni_{12.6}Al_{10}$) or $Cu_{47}Ti_{33}Zr_{11}Ni_8Si_1$ BMG alloy.[1,8]

Zr-based alloy ingots were prepared by arc melting a mixture of pure metal elements (purity 99.9% or greater) in a titanium-gettered argon atmosphere. Unidirectional tungsten wires with a diameter of

about 250 μm were straightened and cut to 5 cm in length, then degreased by ultrasonic cleaning in a bath of acetone followed by the same procedure in a bath of ethanol. The tungsten/BMG composite samples containing 20, 60, and 80 vol % tungsten wires by volume fraction were prepared by melt infiltration casting.[13] The tungsten wires were placed in a quartz tube with an inner diameter of 4 mm and then molten master alloy ingot was infiltrated among them by applying gas pressure. The tube was then quickly removed from the furnace and quenched in a brine solution, and the tungsten/BMG composite samples having uniformly dispersed tungsten wires were prepared. For comparison, monolithic Zr-based BMG was prepared by water quenching. Then the tungsten/BMG composite samples were cut to a length of 7 mm and etched by the electrochemistry method in a sodium hydroxide electrolyte (5–10 wt %) operated at voltage of 12 V. The composite specimens were clamped on a stainless steel specimen holder and two-thirds of the samples were vertically immerged in the electrolyte, and the samples worked as anodic electrode, while a stainless steel plate worked as cathodal electrode. After some time, the tungsten wires in the composite samples were removed and honeycomb porous bulk metallic glass was obtained.

In the case of sodium hydroxide electrolyte, because of the high corrosion resistance of BMG, the cathodal and anodic reactions are as follows

Cathode

$$6H_2O + 6e^- \rightarrow 3H_2 + 6\,OH^- \quad [1]$$

Anode

$$W + 8\,OH^- \rightarrow WO_4^{2-} + 4H_2O + 6e \quad [2]$$
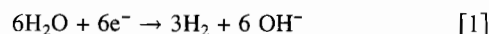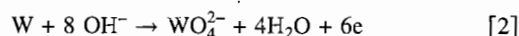
Combining Eq. 1 and 2, we get the following formula

$$W + 2\,OH^- + 2H_2O \rightarrow WO_4^{2-} + 3H_2 \quad [3]$$

The hydrogen gas produced from the cathodal reaction carries the electrolyte upward along with the pores, which are formed during the dissolution of the tungsten wires. This makes the sample in the electrolyte react continuously, and finally the tungsten wires are etched completely. Density is measured by the Archimedian principle. The density of monolithic Zr-based BMG is 6.11 g/cm^3.

X-ray diffraction (XRD) analyses of the samples were performed using Cu Kα radiation (Rigaku D_{max}-RB). Differential scanning calorimetry (DSC) was performed with a Netzsch DSC 404C differential scanning calorimeter under argon atmosphere. A constant heating rate of 20 K/min was employed. A Zeiss Supra 55 scanning electron microscope was used to examine the cross-sectional morphologies of the porous bulk metallic glasses. Compressive testing was performed under displacement control at a constant displacement rate of 5×10^{-4} s^{-1} on a CMT4305 mechanical testing apparatus.

z E-mail: drzhangy@skl.ustb.edu.cn
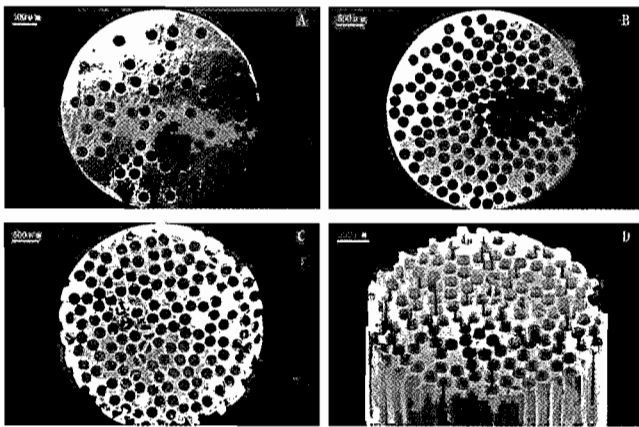
Figure 1. SEM images of the cross sections of porous Zr-based BMGs with nominal porosities of (A) 20, (B) 60, and (C) 80 vol %, respectively. A side view of (C) is shown in (D), illustrating the unidirectional pore structure.

Scanning electron microscopy (SEM) images of the porous Zr-based BMGs with nominal 20, 60, and 80 vol % porosities are shown in Fig. 1. The pores in the PMGs are macroscopically homogeneous and honeycomb-shaped (Fig. 1A-1C) and the size of the individual pore is about 250 μm in diameter. A side view of Fig. 1C is shown in Fig. 1D, illustrating the unidirectional pore structure.

The amorphous structure of the porous Zr-based BMG was identified by XRD. The XRD pattern taken from the cross section of the PMG with 60 vol % porosity is shown in Fig. 2. For comparison, XRD patterns taken from the W/Zr-based BMG composite precursor and tungsten wires are also included. Crystalline peaks corresponding to elemental W are presented in the precursor sample, and only a broad diffraction maximum, characteristic of amorphous structure, is observed in the PMG. These results indicate that this PMG is composed of a single amorphous phase. The PMGs with 20 and 80% porosities show the same characteristics.
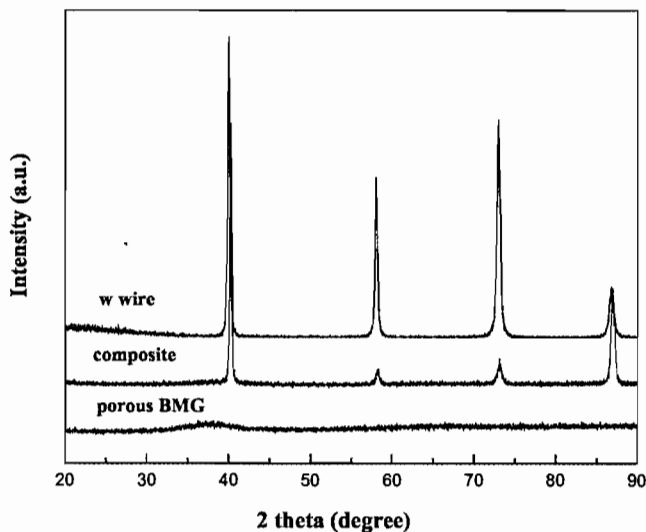
The DSC curve of the porous Zr-based BMG with 60 vol % porosity at the heating rate of 20 K/min under argon is shown in Fig. 3, together with the data of the monolithic Zr-based (pore-free) sample prepared by water quenching. The thermogram of the porous alloy exhibits a glass transition endotherm (onset at T_g) and a crys-
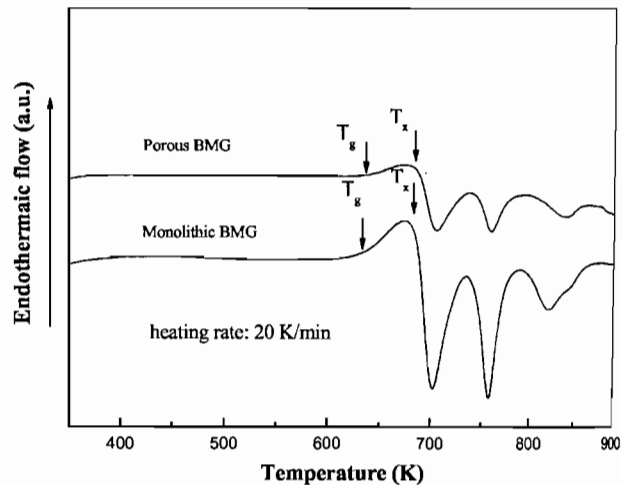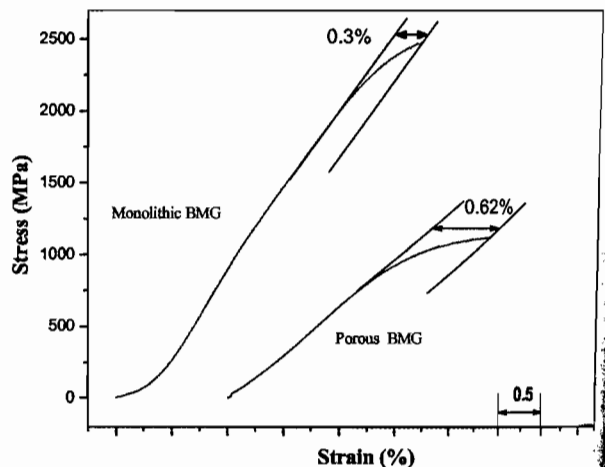

Figure 3. DSC trace of the porous Zr-based BMG with porosity of 60 vol %, showing a glass transition at 638 K followed by crystallization. The data of the monolithic Zr-based BMG prepared by water quenching is shown for comparison.

tallization exotherm (onset at T_x) appearing at 638 and 688 K, respectively, in agreement with those of the monolithic sample.

The typical compressive engineering stress-strain curve of the honeycomb porous Zr-based BMG with the porosity of 60 vol % is shown in Fig. 4, together with the data of the pore-free alloy prepared by water quenching. The porous alloy is more ductile and softer than the pore-free counterpart. The yield strength ($\sigma_{0.2}$) is about 820 and 2000 MPa for the porous and pore-free BMG, respectively. The corresponding yield strain is 1.3 and 1.7%, respectively. The porous sample exhibits a plastic strain of 0.6% before failure, while the value of the pore-free sample is only 0.3%. A SEM micrograph depicting the shear bands forming and then arrested by the fibrous channel during compressive deformation for the porous Zr-based BMG with a porosity of 60 vol % is shown in Fig. 5. Brothers pointed out that pores in porous metallic glass may confine shear-band propagation and increase shear-band densities by arresting the small number of bands normally responsible for compressive failure in monolithic bulk metallic-glass samples, in much the same way that reinforcing metallic or ceramic phases enhance compressive ductility in amorphous metal-matrix composites, and that improvements in ductility through introduction of low (<70%) porosity

Figure 2. XRD pattern taken from the cross section of the porous Zr-based BMG with porosity of 60 vol %. For comparison, XRD patterns taken from the W/Zr-based BMG composite precursor and tungsten wires are included.

Figure 4. Compressive stress-strain behavior of the porous Zr-based BMG with porosity of 60 vol %. The data of the monolithic Zr-based BMG prepared by water quenching is shown for comparison.
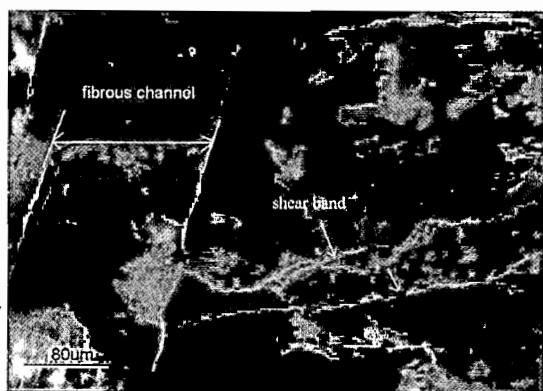
Figure 5. SEM micrograph depicting the shear bands forming and then arrested by the fibrous channel during compressive deformation for the porous Zr-based BMG with porosity of 60 vol %.

levels are probably best rationalized in terms of unstable shear-band arrest.[1] So, the fibrous channel in Fig. 5 confines single shear-band propagation by arresting the small number of shear bands and thus allows the formation of multiple shear bands in the PMG, which promotes stable crack growth and extends the PMG strain to failure.

Using the BMG density data, the specific surface area of the present honeycomb porous BMGs is calculated to be 0.65, 3.96, and 10.54×10^{-3} m^2/g for 20, 60, and 80 vol % porosity, respectively. The whole density of the PMG can be calculated by the following equation

$$\rho_{PMG} = \rho_{BMG}(1 - V_p) \qquad [4]$$

Here, ρ_{PMG} and ρ_{BMG} are the whole density of the porous BMG and the monolithic BMG and V_p is the volume fraction of the porosity. According to Eq. 4, the whole density of the PMG with 80 vol % porosity is about 1.2 g/cm^3, which is a very lightweight material. Furthermore, the size and distribution of pores are controllable by adjusting the diameter and volume fraction of the tungsten wires during melt infiltration. Also, the composite precursor can be selected flexibly; for example, the tungsten wires can be replaced by copper wires.[14]

References

1. A. H. Brothers, *Scr. Mater.*, **54**, 513 (2006).
2. S. Hiromoto, K. Asami, A. P. Tsai, and T. Hanawa, *Mater. Trans.*, **43**, 261 (2002).
3. J. Schroers, C. Veazey, and W. L. Johnson, *Appl. Phys. Lett.*, **82**, 370 (2003).
4. T. Wada and A. Inoue, *Mater. Trans.*, **44**, 2228 (2003).
5. A. H. Brothers and D. C. Dunand, *Adv. Mater. (Weinheim, Ger.)*, **17**, 484 (2005).
6. A. H. Brothers and D. C. Dunand, *Appl. Phys. Lett.*, **84**, 1108 (2004).
7. J. Jayaraj, B. J. Park, D. H. Kim, W. T. Kim, and E. Fleury, *Scr. Mater.*, **55**, 1063 (2006).
8. M. H. Lee and D. J. Sordelet, *Scr. Mater.*, **55**, 947 (2006).
9. J. Banhart, *Prog. Mater. Sci.*, **46**, 559 (2001).
10. A. Inoue, *Acta Mater.*, **48**, 279 (2000).
11. M. L. Kai Hoa, M. Lu, and Y. Zhang, *Adv. Colloid Interface Sci.*, **121**, 9 (2006).
12. H. Nakajima, *Prog. Mater. Sci.*, **52**, 1091 (2007).
13. R. B. Dandliker, R. D. Conner, and W. L. Johnson, *J. Mater. Res.*, **13**, 2896 (1998).
14. P. Wadhwa, J. Heinrich, and R. Busch, *Scr. Mater.*, **56**, 73 (2007).